11th International Symposium on Turbulence and Shear Flow Phenomena (TSFP11)
Southampton, UK, July 30 to August 2, 2019

DYNAMICS OF NATURAL AND PERTURBED TURBULENT SEPARATION BUBBLES

Wen Wu
Department of Mechanical Engineering
Johns Hopkins University
3400 N Charles St, Baltimore, MD 21218
w.wu@jhu.edu

Charles Meneveau
Department of Mechanical Engineering
Johns Hopkins University
3400 N Charles St, Baltimore, MD 21218
meneveau@jhu.edu

Rajat Mittal
Department of Mechanical Engineering
Johns Hopkins University
3400 N Charles St, Baltimore, MD 21218
mittal@jhu.edu

ABSTRACT

Separation of a fully-developed turbulent boundary layer over a flat plate is studied by direct numerical simulation. A massive separation is induced in a $Re_\theta = 490$ turbulent boundary layer by imposing a transpiration velocity profiles at the top boundary of the computational domain. Comparisons are made between steady and time-varying suction-blowing transpiration velocity profiles, as well as a profile with a steady, single suction peak. The latter produces an inviscid pressure gradient at the wall that is qualitatively similar to the one over an airfoil at large angle-of-attack. Particular attention is given to the unsteadiness of the turbulent separation bubble. The time-periodic modulation of the freestream pressure gradient ranges over $\pm 25\%$ of the natural frequency of the separation bubble. The blowing followed by suction creates a forced reattachment that limits the development of the separated shear layer so that even perturbing the freestream pressure gradient does not significantly affect the mean separation bubble. With only suction, the flow reattaches as the separated shear layers grows by turbulent diffusion of momentum, leading to a much longer mean separation bubble. The separation bubble also exhibits significant unsteadiness both at the wall and in the separated shear layer, at two distinct frequencies. Implications for possible mechanisms underlying the two unsteady modes are discussed.

1 Introduction

Turbulent separation bubbles (TSBs) are ubiquitous in external as well as internal aerodynamic systems. The unsteadiness in velocity and pressure that is associated with TSBs can lead to vibration, noise, and even unsteady thermal loads. They also introduce difficulties for prediction, but might also offer opportunities for active and passive control of these flows. A better understanding of the physics of TSB is therefore required to improve the capability of modeling and eventually controlling the unsteady aspects of these flows in technological applications.

One feature of these flows that has received considerable attention is the presence of two distinct and significant unsteady modes that lead to variations in TSB size of up to 90%: a low frequency "breathing" or "flapping" mode ($St \sim 0.01$) (Mohammed-Taifour & Weiss, 2016) and a high frequency "shedding" mode ($St \sim 0.35$) (Na & Moin, 1998; Mohammed-Taifour & Weiss, 2016; Wu & Piomelli, 2018). While the high frequency mode is generally considered to be associated with the vortex generation in the shear layer, the cause of the low-frequency unsteadiness at a time-scale significantly larger than the convective time-scale corresponding to the bubble is still unclear. Note that, large-scale unsteadiness is observed in a wide range of configurations that produce flow separation. For geometry-induced flow separation, for example, researchers have examined flow separation at the leading edge of a blunt flat plate (Cherry *et al.*, 1984), at the sharp corner of a back-facing step (Eaton, 1982) or a diffuser (Kaltenbach *et al.*, 1999), and around a hump (Marquillie & Ehrenstein, 2003) or bluff body (Najjar & Balachandar, 1998).

High-fidelity numerical simulation provides a fruitful way to investigate the mechanisms responsible for generating such modes. In particular, in simulations it is feasible to perturb the TSB in a controlled manner to dissect the nonlinear dynamics associated with the unsteady mode. For pressure induced TSBs over a flat plate (in which the surface curvature is removed), however, simulations have not yet reproduced the low frequency unsteadiness. The specific focus of this work is to explore the flow-physics underlying the appearance and scaling of distinct time-scales observed in an adverse pressure-gradient (APG) induced TSBs which is devoid of configuration-dependent curvature effects. The particular objective here is to gain insights into the flow physics required for the development of efficient passive and active control strategies.

In the next section, the problem setup will be described, and the boundary conditions and numerical method will be presented. We will then present an analysis comparing the separated shear layer with a canonical plane mixing layer, and discuss the mean flow statistics. We will then focus on the effects of time-periodic modulation the freestream pressure gradient. Finally, a new configuration that promotes the low-frequency unsteadiness will be discussed.

2 Methodology

Incompressible Navier-Stokes equations are solved using a well-validated, in-house finite difference code ViCar3D (Mittal *et al.*, 2008; Wu *et al.*, 2018). Separating turbulent boundary layers over a flat plate are investigated at Re_θ = 500. The computational domain is shown in Figure 1. The scales used for normalization are the freestream velocity, $U_o = U_\infty(x = 0)$ and the momentum thickness, $\theta_o = \theta(x = 0)$, at a reference plane in the zero-pressure-gradient region. The recycling and rescaling method of Lund *et al.* (1998) together with the constant spanwise shift proposed by Munters *et al.* (2016), is used at the inlet, while a convective boundary condition is used for the outlet. The recycling region ranges from x = -220 to -120θ_o.

A closed turbulent separation bubble is formed by imposing a suction-blowing vertical velocity distribution at the top boundary to produce an adverse-to-favourable pressure gradient (Na & Moin, 1998; Abe, 2017). The suction starts far away of the recycling plane at x=0, which is about twenty times the boundary layer thickness downstream. The streamwise velocity at the top boundary satisfies the zero mean vorticity condition. To gain insights into the natural time-scales of these bubbles we also vary the pressure gradient in time. 2304, 408 and 384 grid points are used in the streamwise (x), wall-normal (y) and spanwise (z) directions, respectively. The grid resolution at the reference plane is $\Delta x^+ = 9$, $\Delta z^+ = 7$ and $\Delta y_1^+ = 0.6$. Compared with the Kolmogorov scale η, the present resolution gives $\Delta x/\eta \leq 1.3$, $\Delta z/\eta \leq 1.1$ and $\Delta h/\eta \leq 2$ (where $\Delta h = \sqrt{\Delta x^2 + \Delta y^2 + \Delta z^2}$). Since the maximum dissipation of turbulence occurs at a length scale of about 24η (Pope, 2000), the present grid is able to resolve a substantial part of the dissipation spectrum. Statistics are collected over 10,000 time units after the flow reaches the statistical steady state. Simulations have been validated by comparing with Abe (2017).

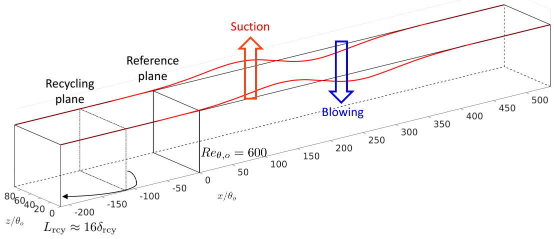

Figure 1. Computational domain

3 Results

The separation bubble is found to naturally oscillate at a Strouhal number $St \equiv fL_{\text{sep}}/U_\infty \approx 0.42$ ($f \approx 0.0028U_\infty/\theta_o$), which is close to the value of the shedding mode reported in previous studies (Na & Moin, 1998; Abe, 2017; Mohammed-Taifour & Weiss, 2016). The time history of the surface area of the backflow region in an $x-z$ plane in the vicinity of the bottom surface (Fig. 8 (a)) is plotted in Fig. 8 (b). The root-mean-square of the fluctuation is $\Delta A_{\text{rms}} \approx 32L_z$ (L_z denotes the size of the calculation domain in the spanwise direction) indicating a significant (20%) change with time compared to the average bubble (length $L_s = 150\theta_o$). Applying conditional averaging at times when this area is at its minimum or maximum value, the phase-averaged mean velocity is obtained and compared in Fig. 8 (c). It can be seen that near the reattachment point ($x \approx 320$), the separating shear layer flaps upstream when the bubble is at its minimum size (dashed lines, compared with the solid lines which denote the state of the largest bubble), and the backflow in the rear end of the bubble (x=[250,270]) is stronger. Meanwhile, the backflow inside the leading part of the separation bubble (x=[180,220]) is weaker. The uphill-side of the separation bubble does not change much between the two states. These observations indicate that the smallest bubble occurs when the 'tail' of the shear layer impinges more vertically to the surface, causes more fluid to be deflected upstream and added to the backflow inside the bubble, and then leads to the subsequent enlargement of the bubble. It supports the imbalanced entrainment (by shear layer) and reinjection (near reattachment) mechanism that has been proposed in previous studies to explain the unsteadiness in laminar separation bubble (Eaton, 1982).

We examined details of the separating shear layer by transforming the velocity fields to the streamline coordinates. It is found that the velocity in the cross-stream direction can be scaled very well by $(U_s - \langle U_s \rangle)/\Delta U_s$ and d_n (where subscripts $()_s$ and $()_n$ denote the directions tangential and perpendicular to the streamline, respectively; and $\langle U_s \rangle$ (ΔU_s) the average (difference) of the peak-magnitude U_s along $\vec{n}$ at the two sides of the shear layer). The frequency found from the periodicity of the backflow area agrees with the natural vortex shedding frequency of a mixing layer $St_{\delta_\omega} \equiv f\delta_\omega/\langle U_s \rangle = 0.2$ (Fig. 2), indicating that the separating layer is similar to a plane

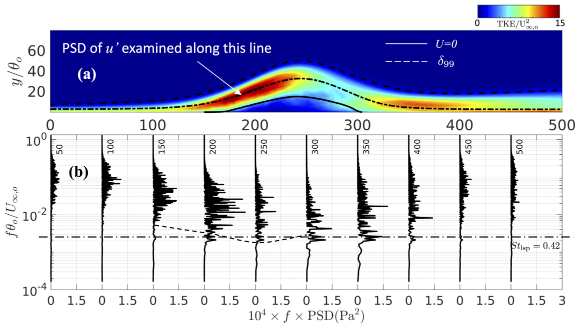

Figure 2. (a) Contour plot of TKE. (b) Power-spectral density of u' examined at several locations along the dot-dashed streamline in (a). Dashed line in (b), vortex shedding frequency of the mixing layer; dot-dashed line, the observed oscillating frequency.

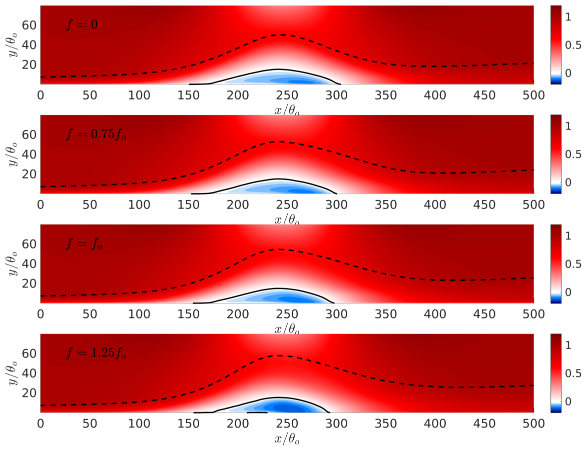

Figure 3. Mean velocity obtained by steady and perturbed TSB. Dashed, δ_{99}; solid, U=0.

mixing layer driven by the Kelvin-Helmholtz instability. Coincidentally, the time-scale that a fluid elements travels around the separation bubble is also close to the time-scale characterizing the bubble oscillation. It has been proposed in previous studies that the mode at $St = 0.35$ is related to the shedding of large-scale turbulent structures in the separating shear layer (Na & Moin, 1998; Abe, 2017). The footprints of large-scale, quasi-two-dimensional outer layer structures can be observed in the near-wall flow shown in Fig. 8 (a). At this point, however, we cannot conclude if it is the shedding time-scale or the passage time-scale that determines the unsteady mode because the scale-separation between the two is quite small in this case. Despite the similarity, the separating shear layer exhibits counter flow and thus differs from canonical mixing layers more typically formed by co-flowing streams. Moreover, in our case the velocity ratio $R = (U_1 - U_2)/(U_1 + U_2)$ (subscripts denote the two sides of the shear layer) exceeds the threshold of 1.315 that separates convective and global instability in laminar shear layers (Huerre & Monkewitz, 1985), between x=245 and 275, indicating the possible existence of a global instability in this flow. And, unlike the plane mixing layer under a ZPG, the separating shear layer is still affected by the freestream pressure-gradient, especially adverse PG conditions near the reattachment point.

We performed three additional simulations in which the PG is modulated by ±20% around its local steady value in time. The frequencies of the variation are 0.75, 1.0 and 1.25 of the natural shedding frequency observed in the steady PG case. It is found that the size of the mean separation bubble dose not change much between the cases (Figure 3). The magnitude of the backflow inside the bubble increases slightly with the modulation frequency. The magnitude of turbulent kinetic energy (TKE) in the high-TKE region in the uphill-side of the separation bubble is increased by the modulation. In particular, the TKE is amplified most significantly when the modulation frequency is equal to the natural shedding frequency.

4 Suction-only simulation

The small change of the TSB due to the variation of the freestream pressure gradient is unexpected. We noticed that the suction-and-blowing configuration generates an APG followed by an FPG and the latter leads to a forced reattachment of the flow. However, natural separating flow such as on airfoils and in diffusers do not have this type of forced FPG driven reattachment and we expect that this would also impact the any low frequency modes (breathing/flapping) modes that involve the opening and closing of the bubble. Motivated by these expectations, we simulated a suction only (APG only) induced separation bubble at the same Reynolds number.

The velocity profile used at the aspirated top boundary is showed in Figure 4 and compared with the suction-and-blowing cases. The suction-and-blowing configuration produces a bell-shape inviscid wall pressure profile over the surface that consists of an APG followed by an FPG. Pressure profiles of realistic separated flow are however, quite different. For an airfoil at large angle-of-attack, a steep APG appears near the leading of the airfoil and gradually decreases towards the trailing edge. However, there is usually no region of FPG (Rinoie & Takemura, 2004). In diffusers (Kaltenbach *et al.*, 1999) for example, a strong APG occurs at the beginning of the deflected wall and decreases rapidly to a ZPG downstream.

To mimic a more realistic pressure gradient in these applications, we use an inviscid pressure profile over the suction surface of NACA 0012 airfoil at a six degree angle-of-attack as a guide to obtain a suction velocity profile on the top surface. We employ a two-dimensional, inviscid solver for our rectangular computational domain and use an iterative approach to adjust the free parameters of a Gaussian profile. Note that a similar single suction peak configuration has been used in a few previous studies on laminar separation bubbles (Spalart & Strelets, 2000). The pressure gradient obtained by the optimized suction-only profile reproduces the pressure gradient over the airfoil very well (Figure 4). Note that the calculation

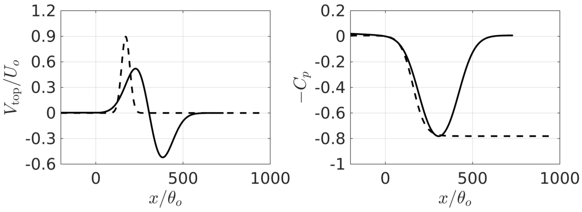

Figure 4. Profiles of (a) the vertical velocity at the top boundary and (b) inviscid C_p at the bottom boundary. solid, suction-blowing; dashed, suction-only.

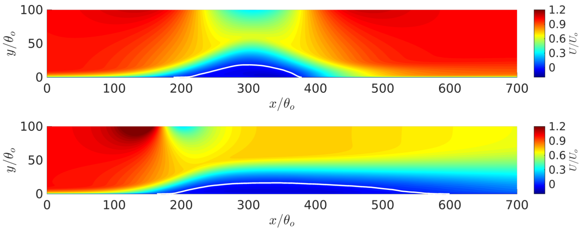

Figure 5. Mean streamwise velocity with contour line $U = 0$ (solid). Top, suction-blowing; bottom, suction only.

domain is much longer in x for this case because the mean separation bubble is significantly longer than the one in the suction-blowing case (Figure 5).

Snapshots of the instantaneous vortex structures in the two separation bubbles with a steady freestream PG are showed by the second invariant of the velocity-gradient tensor $Q = -\frac{\partial u_j}{\partial x_i}\frac{\partial u_i}{\partial x_j} = \frac{1}{2}\left(\Omega_{ij}\Omega_{ij} - S_{ij}S_{ij}\right)$ where Ω_{ij} and S_{ij} are the antisymmetric and symmetric parts of the velocity gradient tensor respectively. It can be seen that many streamwise elongated low-speed regions surrounded by a group of hairpin-like structures are present in the separated shear layer. The size of these streaks in the spanwise direction is relatively small near the separation point and they merge into larger structures as the flow separates. When the blowing is applied at the top boundary, these streamwise vortices are broken by it and near-wall streaks form during its recovery to turbulent boundary layer after reattachment. Without the blowing, on contrary, these structures in the separated shear layer sustain for a long time and break around $x = 450\theta_o$ at the time-instant shown. A large vorticity packet is observed downstream with nests of small-scale turbulent eddies. The difference in the mean velocity and turbulent structures indicates change of the turbulence development between suction-blowing and suction-only. In particular, the anisotropy of the turbulence exhibits significant differences between the two configurations (fig. 9): the forced blowing causes an abrupt change in the flow direction near the crest of the separation bubble and breaks up all coherent structures; the flow experiences suppression of u' due to impingement before reattaching and rapidly recovering towards a canonical TBL downstream. Without the blowing, the separated shear layer develops more naturally and does not recover to TBL within the present computational domain.

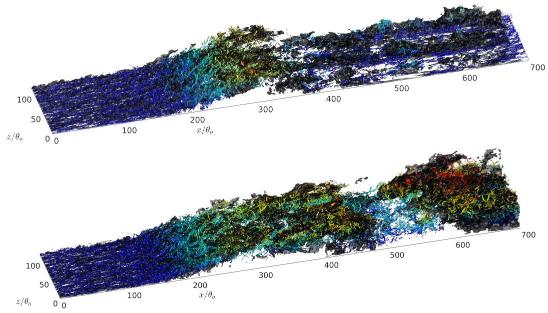

Figure 6. Instantaneous vortex structures of TSB for: top, suction-blowing; bottom, suction only, visualized by the isosurfaces of Q (see text) colored by the distance from the wall. The dark-gray isosurfaces are $u' = -0.1U_o$.

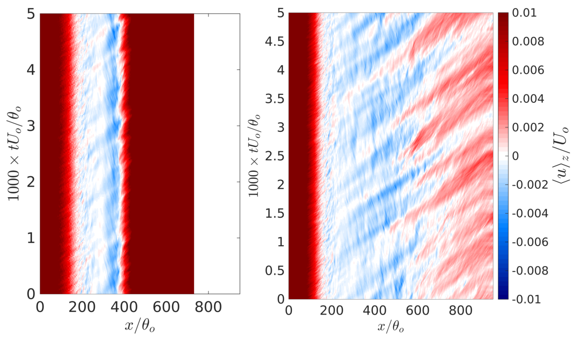

Figure 7. Spatial-temporal map of the spanwise-averaged streamwise velocity at the first grid point away from the bottom wall. Left, suction-blowing; right, suction only.

The spatial-temporal map of the spanwise-averaged streamwise velocity in the vicinity of the wall is plotted in Fig. 7. Without blowing, besides the fluctuation of the incoming turbulent boundary layer at very small time scales, a high frequency unsteadiness is can be discerned as parallel blue stripes, separated in time by about $TU_o/\theta_o \approx \mathcal{O}(400)$ in the map. At a larger time scale of $TU_o/\theta_o \approx \mathcal{O}(1000)$, strong forward flows are observed to penetrate into the reverse flow region up to $x/\theta_o = 400$. The two unsteady phenomena appear as highly stochastic, thus the time scales mentioned above are only representative order of magnitude values. It is noticeable that the low frequency mode does not appear in the suction-blowing case, in which the reversed flow stripes exhibit approximately the same temporal displacements near the separation and reattachment regions.

Similar frequency peaks and scale separations are also observed in the separated shear layer. Figure 10 shows the pre-multiplied energy spectra of pressure fluctuations examined at several locations within the high TKE regions. The peaks of the spectra agree well with the frequency seen in the time history of reversed flow on the wall. Recall that the closed separation bubble created by suction-blowing shows a shedding frequency at $f = 0.0028U_o/\theta_o$, which barely changes when we remove the blowing. So we conclude that the front part of the TSB is well described by the mixing layer relation and the high frequency mode corresponding to generation of roller vortices in the separated shear layer. The low-frequency mode, on the other hand, seems to be related the break up of the vortex train and merging of vorticity.

5 Conclusions

In this study, we investigated a turbulent separation bubble created on a flat plate by freestream pressure gradients. The observations on the shedding mode at $St = 0.42$ agree well with previous studies. Forcing the bubble at different frequencies shows that the mean separation bubble is constrained by the imposed suction-blowing flow and turbulence is slightly amplified when the freestream pressure gradient oscillates at the natural frequency of the bubble. Once the favourable pressure gradient generated by the blowing is removed, the separated flow is allowed to develop more freely and it reattaches via turbulent diffusion much further downstream. With this change in the configuration, a low-frequency unsteady mode is observed in addition to the vortex shedding mode and is associated with the quasi-periodic formation of large vorticity packets. The shedding mode has similar frequency with or without the blowing, around $f = 0.0025\theta_o/U_o$ and is well characterized by the most unsteady mode of a plane mixing layer. The corresponding Strouhal number $St_l = fL_{sep}/U_o$ is 0.42 and 1.00 for the suction-blowing and suction-only cases, respectively, showing that this parameter may not be a good universal measurement to categorize the unsteadiness by a physical interpretation. The low frequency motion occurs at $f = 0.001\theta_o/U_o$ and is most evident in the rear part of the separation bubble. Flow visualizations and further analysis indicate that the motion is associated with a breakup of a vortex train in the separated shear layer and the subsequent formation of discrete vorticity packets. The mechanism of the low-frequency motion is presently under study.

6 Acknowledgement

The authors acknowledge the support from AFOSR Grant FA9550-17-1-0084, monitored by Dr. Gregg Abate. The simulations were performed at the Maryland Advanced Research Computing Centre (MARCC) and the Texas Advanced Computing Center (TACC) Stampede 2 clusters.

REFERENCES

Abe, H. 2017 Reynolds-number dependence of wall-pressure fluctuations in a pressure-induced turbulent separation bubble. *J. Fluid Mech.* **833**, 563–598.

Cherry, N. J., Hillier, R. & Latour, M. E. M. P. 1984 Unsteady measurements in a separated and reattaching flow. *J. Fluid Mech.* **144**, 13–46.

Eaton, J. K. and Johnston, J. P. 1982 Low frequency unsteadyness of a reattaching turbulent shear layer. In *Turbul. Shear Flows* (ed. F. Bradbury, L. J. S. and Durst, Launder B. E. & Schmidt F. W. and Whitelaw J. H.), pp. 162–170. Berlin, Heidelberg: Springer.

Emory, M. & Iaccarino, G. 2014 Visualizing turbulence anisotropy in the spatial domain with componentality contours. In *Center for Turbulence Research. Annual Research Briefs*, pp. 123–138.

Huerre, P. & Monkewitz, P. A. 1985 Absolute and convective instabilities in free shear layer. *J. Fluid Mech.* **159**, 151–168.

Kaltenbach, H. J., Fatica, M., Mittal, R., Lund, T. S. & Moin, P. 1999 Study of flow in a planar asymmetric diffuser using large-eddy simulation. *J. Fluid Mech.* **390**, 151–185.

Lund, T., Wu, X. & Squires, K. 1998 Generation of turbulent inflow data for spatially-developing boundary layer simulations. *J. Comput. Phys.* **140**, 233258.

Marquillie, M. & Ehrenstein, U. 2003 On the onset of nonlinear oscillations in a separating boundary-layer flow. *J. Fluid Mech.* **490**, 168–188.

Mittal, R., Dong, H., Bozkurttas, M., Najjar, F., Vargas, A. & von Loebbecke, A. 2008 A versatile sharp interface immersed boundary method for incompressible flows with complex boundaries. *J. Comp. Phys.* **227** (10), 4825–4852.

Mohammed-Taifour, A. & Weiss, J. 2016 Unsteadiness in a large turbulent separation bubble. *J. Fluid Mech.* **799**, 383412.

Munters, M, Meneveau, C. & Meyers, J. 2016 Shifted periodic boundary conditions for simulations of wall-bounded turbulent flows. *Phys. Fluid* **28** (2), 025112.

Na, Y. & Moin, P. 1998 Direct numerical simulation of a separated turbulent boundary layer. *J. Fluid Mech.* **370**, 175–201.

Najjar, F. M. & Balachandar, S. 1998 Low-frequency unsteadiness in the wake of a normal flat plate. *J. Fluid Mech.* **370**, 101–147.

Pope, S. B. 2000 *Turbulent Flows*. Cambridge University Press.

Rinoie, K. & Takemura, N. 2004 Oscillating behaviour of laminar separation bubble formed on an aerofoil near stall. *Aeronau. J.* **108**, 153–163.

Spalart, P. R. & Strelets, M. KH. 2000 Mechanisms of transition and heat transfer in a separation bubble. *J. Fluid Mech.* **403**, 329–349.

Wu, W. & Piomelli, U. 2018 Effects of surface roughness on a separating turbulent boundary layer. *J. Fluid Mech.* **841**, 552–580.

Wu, W., Seo, J.-H., Meneveau, C. & Mittal, R. 2018 Response of a laminar separation bubble to forcing with zero-net mass flux jets. In *Proc. Flow Control Conf., AIAA AVIATION Forum, (2018-4018).*

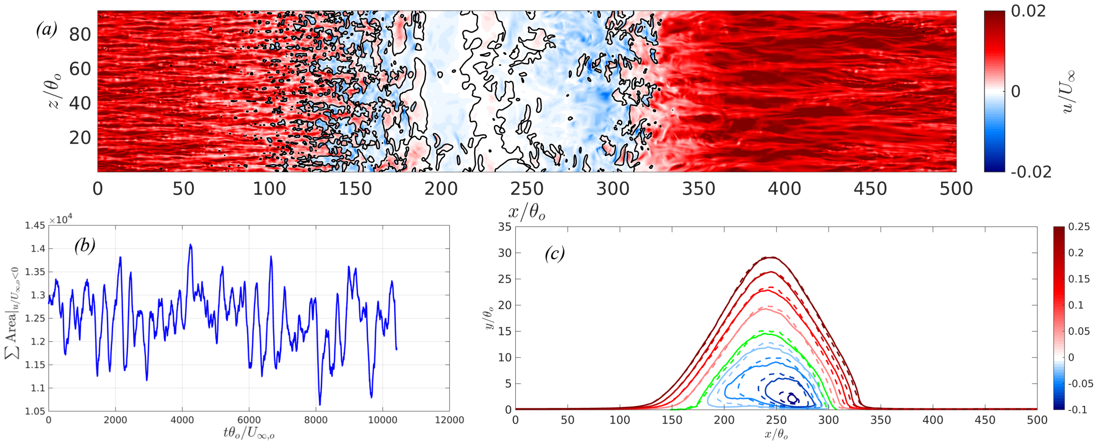

Figure 8. (a) Instantaneous streamwise velocity in the $x-y$ plane at the first grid point away from the bottom wall; (b) time history of total area of backflow region in the near-wall plane; (c) selected contour lines of the phase-averaged streamwise velocity. Solid lines in (a), $u = 0$. In (c), solid lines, bubble at its largest size (*i.e.*, peaks in (b)); dashed lines, bubble at its smallest size. Green solid line shows mean $U = 0$.

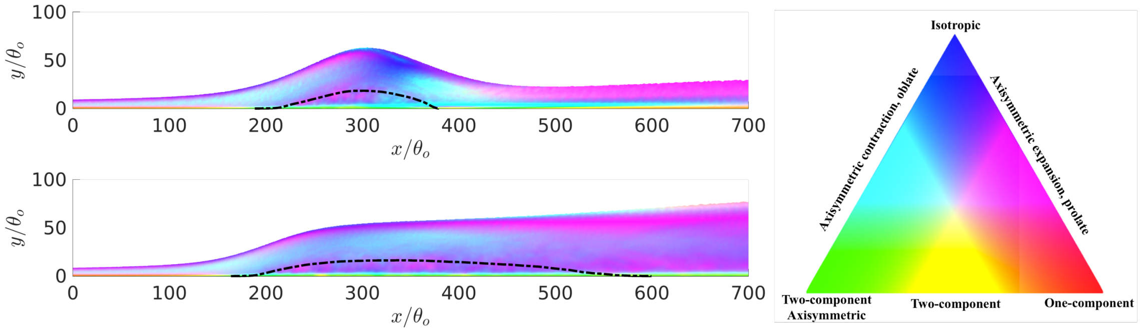

Figure 9. Anisotropy componentality contours (Emory & Iaccarino, 2014) for the TSB up to the edge of the boundary layer. Top, suction-blowing; bottom, suction only. Colored by the regimes shown in the right map.

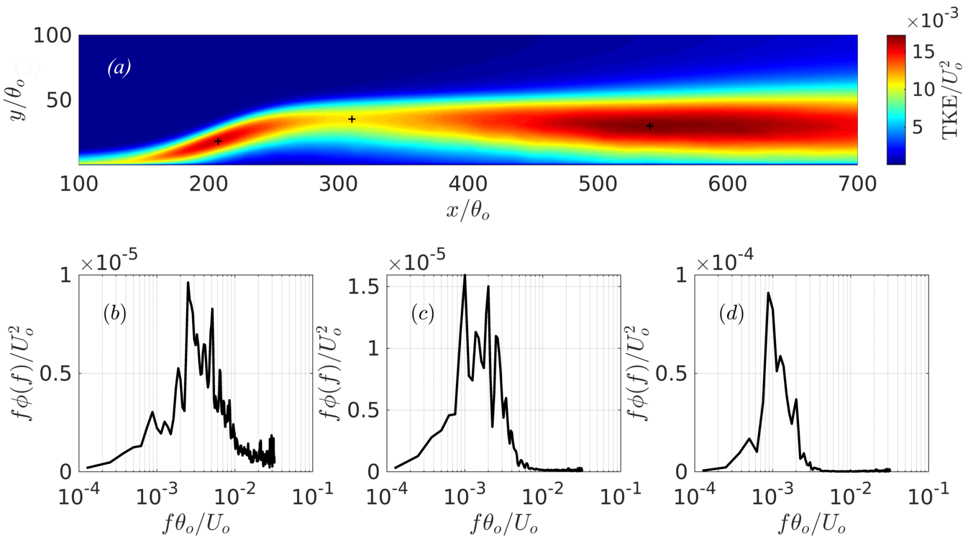

Figure 10. TKE and pre-multiplied energy spectrum of the pressure fluctuation within the separated shear layer of the suction-only case. (a) Contour of TKE. The cross markers indicate the locations where the spectra are obtained. (b-d) the pressure spectrum.